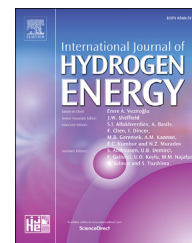




ELSEVIER

Available online at www.sciencedirect.com

ScienceDirect

journal homepage: www.elsevier.com/locate/hydro

Freeze-dried ammonia borane-polyethylene oxide composites: Phase behaviour and hydrogen release



A.R. Ploszajski ^{a,*}, M. Billing ^a, A.S. Nathanson ^a, M. Vickers ^a,
S.M. Bennington ^b

^a Department of Chemistry, University College London, 20 Gordon Street, London, WC1H 0AJ, UK

^b Krino Partners Ltd, 8 King Edward Street, Oxford, OX1 4HL, UK

ARTICLE INFO

Article history:

Received 31 July 2017

Received in revised form

22 November 2017

Accepted 19 January 2018

Available online 21 February 2018

Keywords:

Ammonia borane

Polyether

Hydrogen storage

Hydrogen generation

Dehydrogenation

Phase diagram

ABSTRACT

A solid-state hydrogen storage material comprising ammonia borane (AB) and polyethylene oxide (PEO) has been produced by freeze-drying from aqueous solutions from 0% to 100% AB by mass. The phase mixing behaviour of AB and PEO has been investigated using X-ray diffraction which shows that a new ‘intermediate’ crystalline phase exists, different from both AB and PEO, as observed in our previous work (Nathanson et al., 2015). It is suggested that hydrogen bonding interactions between the ethereal oxygen atom (–O–) in the PEO backbone and the protic hydrogen atoms attached to the nitrogen atom (N–H) of AB molecules promote the formation of a reaction intermediate, leading to lowered hydrogen release temperatures in the composites, compared to neat AB. PEO also acts to significantly reduce the foaming of AB during hydrogen release. A temperature-composition phase diagram has been produced for the AB-PEO system to show the relationship between phase mixing and hydrogen release.

© 2018 The Author(s). Published by Elsevier Ltd on behalf of Hydrogen Energy Publications LLC. This is an open access article under the CC BY license (<http://creativecommons.org/licenses/by/4.0/>).

Introduction

Ammonia borane (AB, NH_3BH_3) is a highly promising candidate material to meet the US Department of Energy's targets for portable hydrogen storage systems owing to its excellent gravimetric hydrogen storage capacity of 19.6 wt% H_2 , low dehydrogenation temperatures (compared to other candidates), and encouraging progress in recycling the material [2].

Unfortunately, the commercialisation of AB has been hampered by its low melting point (114 °C [3]) which, when hydrogen is produced at proximate temperatures, results in a waxy foam that is difficult to contain in a practical device. Other solid-state hydrogen storage materials do not suffer

from such effects. Furthermore, an incubation period exists prior to hydrogen release, and volatile by-products ammonia, diborane and borazine are produced alongside hydrogen, which are known to poison the sensitive catalytic components of fuel cells.

To address these issues, researchers have sought to use nanostructuring and nanoconfinement techniques [4–10] and chemical additives such as metal-containing [11–17] and non-metal-containing [18–23] species to modify the hydrogen release properties of AB. Polymer composites stand out as a particularly attractive option, since polymers tend to be cheap, lightweight and easy to form. To date, poly(methyl acrylate) [24], poly(methyl methacrylate) [25], poly(vinyl pyrrolidone) [26] and polyacrylamide [27] have been employed

* Corresponding author.

E-mail address: anna.ploszajski.13@ucl.ac.uk (A.R. Ploszajski).

<https://doi.org/10.1016/j.ijhydene.2018.01.128>

0360-3199/© 2018 The Author(s). Published by Elsevier Ltd on behalf of Hydrogen Energy Publications LLC. This is an open access article under the CC BY license (<http://creativecommons.org/licenses/by/4.0/>).

successfully by combining confinement and chemical interactions between AB and oxygen-containing functional groups within the polymer, albeit with relatively low AB loadings (<50 wt%).

In recent work [1], it was demonstrated that co-electrospinning AB with high molecular weight polyethylene oxide (PEO), produced solid-state hydrogen storage composites with reduced hydrogen release temperatures, no incubation time and suppression of foaming, even in composites containing 75 wt% AB. Furthermore, a distinct crystal phase, different from both pure AB and PEO, was found to form when the two materials are intimately mixed in this way. This new phase was thought to contain significant hydrogen bonding between the protic hydrogen atoms on the nitrogen atom (N–H) in AB, and the ethereal oxygen atom (–O–) in the PEO backbone.

In this paper we present data collected for AB-PEO composites over the full range of compositions to demonstrate the relationship between the phase mixing behaviour of AB and PEO and the hydrogen release observed. We also demonstrate that a freeze-drying method from aqueous solutions can be used to attain the same intimate mixing of AB and PEO as achieved by co-electrospinning, with the added benefits of a robust manner of composite production and great potential for materials manufacture at industrial scales. It is shown that combining AB with PEO in this way eliminates foaming upon hydrogen release. These advances confirm that AB-PEO composites are extremely promising candidates for portable hydrogen storage applications.

Experimental

Materials

The materials used were PEO (molecular weight 2,000,000 Da) from Sigma Aldrich, containing 200–500 ppm butylated hydroxytoluene (BHT) inhibitor, ≤ 1 wt% alkalis and other metals, and 0.8–3.0 wt% SiO₂ impurities and AB from Minal Intermediates (quoted purity 99%). Both were used without further purification.

Composite preparation

AB-PEO composites were prepared with compositions ranging 0–100 wt% AB. Composites will be denoted AB_{*n*} hereafter, where *n* is the weight percentage of AB within the material. To illustrate, a sample denoted as AB10 contains 10 wt% AB and 90 wt% PEO.

To synthesise the composites, PEO powder was mixed with deionised water for 3 days at room temperature using a magnetic stirrer. The solution was divided and the appropriate mass of AB powder added to produce different compositions by weight. These solutions were stirred at room temperature for 2 h, or until the AB was fully dissolved. The samples were then frozen in a laboratory freezer at –18 °C overnight and the water removed by freeze-drying with the condenser at –55 °C, until a chamber pressure below 50 mTorr was achieved. The samples were stored in sealed containers in air prior to use.

Analytical techniques

Thermal analysis was performed using a Mettler-Toledo combined thermogravimetric analysis and differential scanning calorimetry (TGA-DSC) instrument, which was connected to an MKS Cirrus mass spectrometer (MS). Samples were ramp heated under argon between 35 and 200 °C at 1.2 °C/min, which is approximately equivalent to the heating regime used in the nuclear magnetic resonance experiments described below.

Room-temperature (RT) powder X-ray diffraction (PXRD) was done with a Stoe StadiP transmission diffractometer equipped with a Cu X-ray tube run at 40 kV, 30 mA and a Ge 111 monochromating crystal to give K α_1 radiation at $\lambda = 1.54056$ Å. Data were collected with a Dectris Mythen 1 K silicon strip detector scanned from 5° to 40° 2 θ stepped at 0.5° every 20 s. Data steps were 0.015° 2 θ . For indexing the intermediate phase, data were collected from 2° to 32° 2 θ at 20 s per step.

In-situ PXRD was performed using a Rigaku SmartLab X-ray flat-plate Bragg-Brentano diffractometer with a 9 kW rotating Cu anode at 45 kV and 200 mA, monochromated for K α_1 radiation with a double bounce 220 germanium crystal and data collected with a 1D silicon strip detector. Data were collected from 10 to 30° 2 θ with 0.01° steps every 2 °C intervals from 28 °C to 86 °C with a heating ramp between intervals of 2 °C/min. For both RT and *in-situ* PXRD, samples were rotated in the beam to improve powder averaging.

In-situ solid-state ¹¹B proton-decoupled magic angle spinning nuclear magnetic resonance (¹¹B{¹H} SS MAS-NMR) spectra were obtained at the EPSRC UK National Solid-state NMR Service at Durham. The spin rate used was 3 or 6 kHz, depending on the sample, with magnetic field 9.4 T (128.30 MHz). The measurements were two-pulse phase modulated (TPPM) proton decoupled at a field equivalent to approximately 60 kHz. Spectra were recorded at 10 °C intervals from 25 °C to 195 °C, and for the final products once the instrument had cooled to 25 °C at the end of the experiment. The heating rate was 2 °C/min between each measurement temperature step, and the spectra were recorded 8 min apart: 5 min for heating and 3 min for stabilisation.

Results and discussion

Freeze-drying aqueous AB-PEO solutions produces a white, porous, spongy material (Fig. 1). Materials with low AB content are more elastic and porous than those with higher amounts, due to the elasticity of the PEO component and the greater water content of the solution respectively. The plasticity of AB-PEO materials is useful since it permits the pressing, shaping, moulding and extrusion of the material into any form.

Phase mixing behaviour

Further to our previous work [1] the diffraction patterns of freeze-dried synthesised composites (Fig. 2) show three crystallographic phases present at room temperature: tetragonal AB [28], monoclinic PEO [29] and an unknown intermediate phase.



Fig. 1 – AB-PEO composites: AB30 (left) and AB70 (right).

The diffraction pattern for AB30, attributed to the intermediate phase, was assumed to be sufficiently phase-pure to attempt peak-indexing to obtain a unit cell which was done using the programs Crysfire [30] and Ito [31]. Data collection was optimised for indexing. The resultant orthorhombic unit cell was assigned a possible space-group with the program ChekCell [32] and then refined with Le Bail fitting using the program Rietica [33] (Fig. S1), yielding a weighted profile R-factor of 3%. The unit cell and space-group assigned are not

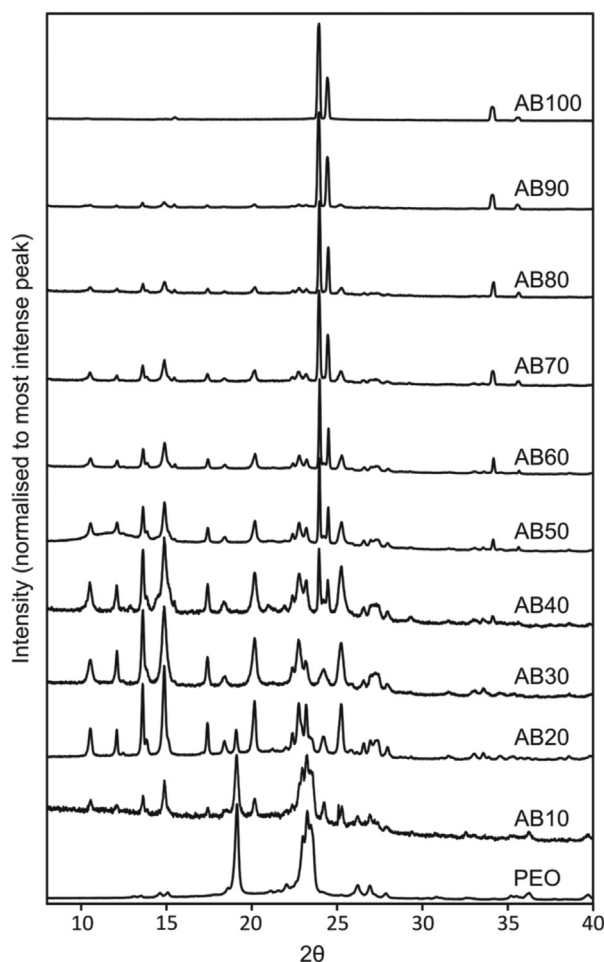


Fig. 2 – Room temperature PXRD patterns for AB-PEO composites from 0% AB (pure PEO) to 100% AB.

unequivocal, but are sufficiently close to model intensities to enable quantitative analysis.

Some of the patterns contain several small peaks from an unidentified phase or phases and are most noticeable in the XRD from AB40. These peaks are also present in the pattern for AB100, so it is likely that they originate from impurities from the as-received AB, or hydrolysis products formed during synthesis. For the Le Bail fits, these regions were excluded from the calculations.

For quantitative analysis of the three phases, the Reference Intensity Ratio (RIR) approach [34] and whole-pattern Le Bail fitting [35] method were used in combination [36]. A RIR is a normalising constant traditionally found by mixing each pure phase with a standard 50% by weight and using the ratio of the strongest diffraction peak measured from standard and phase as a multiplier for the respective strongest peaks of each of the phases in study. This method is prone to large errors due to issues such as preferred orientation of crystals, peak overlap and poor counting statistics. To address this, rather than take a single peak, the individual intensities of all the peaks associated with each phase were calculated and summed. These totalled intensities were calculated by Le Bail fitting the patterns with Rietica using the unit cell and space-group information of each of the phases. Lactose was chosen for the standard as it has similar X-ray absorption properties to that of the analytes. Since only two phases are present in any one material composition the quantitative formula used was for the binary case, (α , β):

$$X_{\alpha} = \frac{C_{\alpha}I_{\alpha}}{C_{\beta}I_{\beta} + C_{\alpha}I_{\alpha}}$$

where X is the weight fraction, and C_{α} the total intensity of the phase α and the constants derived from the 50:50 mix of phase α with the standard. The error was calculated from several preparations and scans of a known weight composition, giving a 2σ of $\approx 4\%$. Plots of the Le Bail fits for these quantitative results are provided in the supplementary section and include the calculated, observed and difference traces (Fig. S2-12).

The resultant composition plot (Fig. 3) shows that the proportion of the intermediate phase increases with increasing AB at the expense of PEO up to AB30, at which point it is phase-pure. From AB40 to AB100, the proportion of AB increases at the expense of the intermediate phase. This method models the relative quantities of the three phases described. Unidentified phases that may be present are excluded.

DSC was employed to observe the behaviour of the phases present in the composites as a function of temperature. There are three distinct endothermic signals in the DSC data consistent with the melting of the three distinct phases (Fig. 4). An endotherm at 68 °C and below corresponds to the melting of PEO, which can only be observed for samples below AB20. An endotherm associated with the melting of the intermediate phase is observed at 74–77 °C for samples between AB30 and AB90. For compositions above AB70, an endotherm at 91–105 °C, typical of AB melting, is evident. The melting of AB is not seen in DSC for compositions AB40-AB60 due to the presence of large exothermic signals from hydrogen release reactions at proximate temperatures.

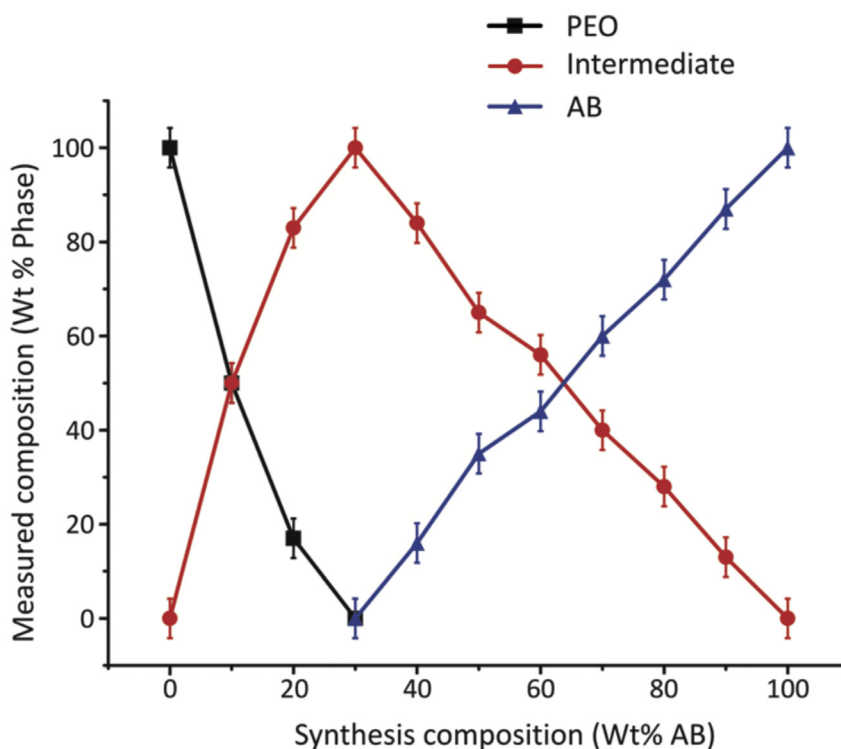


Fig. 3 – Measured proportions of the PEO, intermediate and AB crystalline phases plotted with respect to AB composition.

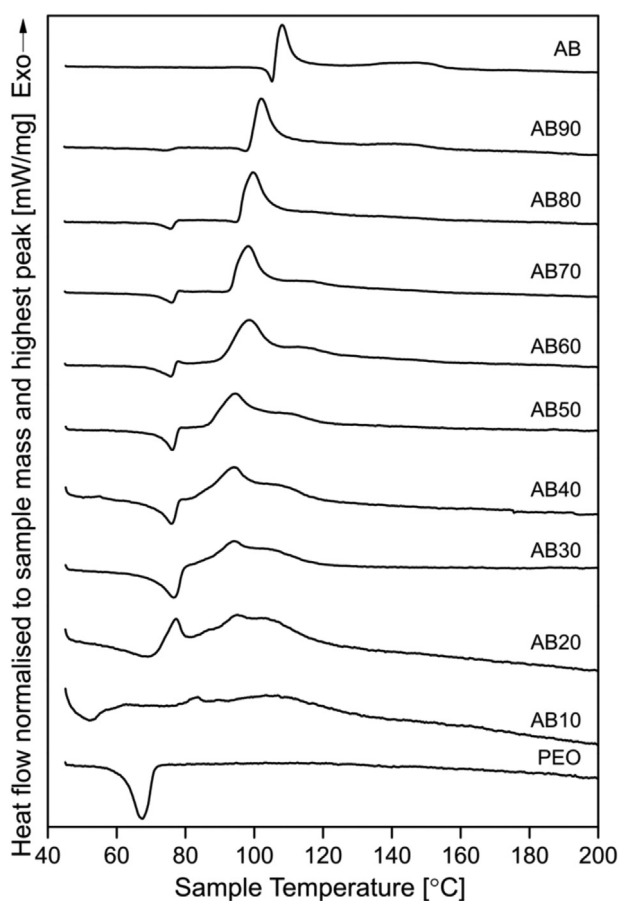


Fig. 4 – DSC data for AB-PEO composites heated at 1.2°C/min, normalised to AB mass and maximum value.

In addition to PXRD and DSC, the boron environments within the composites were probed using $^{11}\text{B}\{^1\text{H}\}$ SS MAS-NMR (Fig. S23), which shows the expected double peak at -25 ppm and -28 ppm, corresponding to BH_3 environments in AB. This complex peak is the result of second order quadrupolar interactions at the low magnetic field used in this work [37]. The shape of the AB peaks change with AB content of the composites, suggesting that mixing AB with PEO changes the quadrupolar environment associated with AB.

In-situ PXRD was used to show the temperatures at which the crystalline phases lose their crystallinity by melting and/or decomposition to amorphous polymeric reaction products following dehydrogenation (Fig. S13-22).

Hydrogen release

Hydrogen release from AB has been studied extensively and is known to occur in the solid-state by thermolysis, an exothermic and step-wise process, in which approximately one molecule of hydrogen per formula unit of AB is released at each step. It has been well-documented using TGA, DSC, MS and volumetric hydrogen release data that the first hydrogen release step occurs between 95°C and 110°C , the second at approximately 130°C and the third at temperatures above 500°C [38,39].

There are two signals in DSC (Fig. 4) and MS data ($m/z = 2$) (Fig. 5) when AB100 is heated to 200°C , which are consistent with the first two accepted hydrogen release steps. Furthermore the hydrogen release events are highly exothermic, in agreement with previous studies. The third hydrogen release step occurs at unfeasibly high temperatures for a practical and efficient working system, so it is not considered in this investigation.

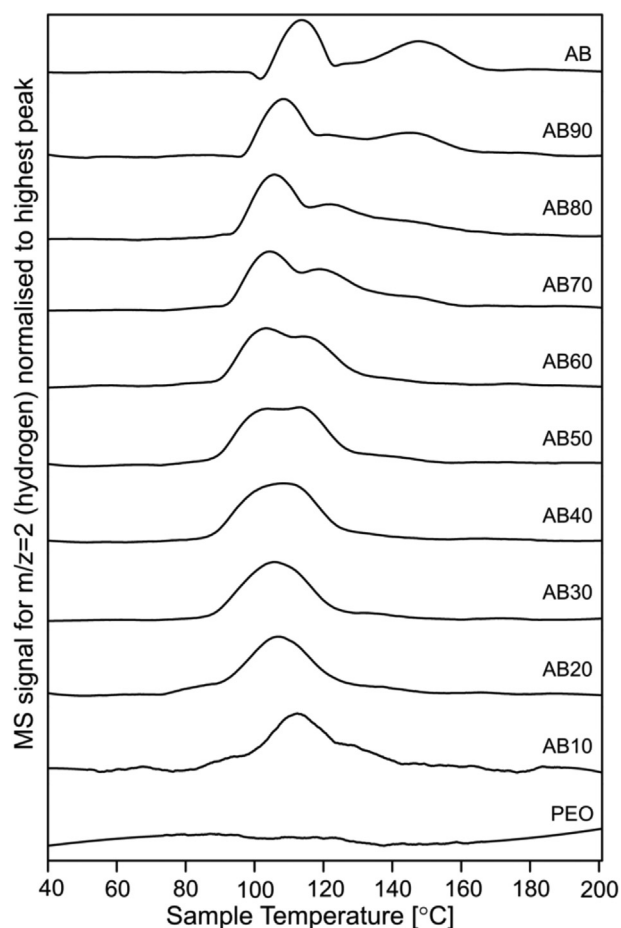


Fig. 5 – H₂ MS data ($m/z = 2$) for AB-PEO composites heated at 1.2 °C/min, normalised to maximum value.

The DSC (Fig. 4) and MS data (Fig. 5) for AB-PEO materials show that the first two hydrogen release steps shift to lower temperatures as the PEO content increases. In fact, the reduction in the hydrogen release temperatures is so pronounced that the exothermic signals overlap with the melting endotherms previously described, such that some endotherms can barely be seen at all.

The temperature difference between the first and second hydrogen release steps also decreases with increasing PEO content, indicating that the activation barrier for this second step of dehydrogenation is significantly reduced in the intermediate phase. Additionally, the intermediate phase exhibits a third, low temperature hydrogen release at ≈ 80 °C (Figs. 4 and 5). This is most prominent in the DSC data for AB20, in which we suspect AB units are only bound with PEO in the intermediate phase. Fig. 3 would suggest that the phase-pure AB30 composition should show the low-temperature hydrogen release in the DSC most prominently, but unfortunately the endothermic melting trough overwhelms the exothermic hydrogen release signal (Fig. 4).

Hydrogen release from AB is known to be accompanied by profuse foaming because it melts prior to hydrogen release, as seen in the DSC data for AB100 (Fig. 4). Bubbles of gas form within the molten material as it rapidly escapes. This represents a serious problem for materials handling in a

commercial system. By ‘foam-testing’, a procedure where 0.1 g pellets are warmed in an oil bath at 120 °C for 3 min, it can be seen that the presence of PEO in the AB-PEO composites significantly reduces foaming during hydrogen release for AB50-AB80 (Fig. 6). The pellets with high PEO content (AB40 and below) have delaminated, possibly because PEO’s elasticity causes spring-back to the original shape when heat is applied.

In addition to the issue of foaming, hydrogen release from AB is accompanied by ammonia, diborane and borazine, which presents a significant problem if AB were to be used to supply hydrogen to a polymer electrolyte membrane hydrogen fuel cell in a functional portable system, because any impurities in the hydrogen gas stream will poison the fuel cell’s sensitive catalytic components.

The release of impurities from AB-PEO materials can be deduced from the TGA data (Fig. S25), because the mass loss from the samples is greater than the amount which would be expected for hydrogen alone, consistent with previous literature. The relative amounts of ammonia, diborane and borazine gases released were measured by MS ($m/z = 17$, $m/z = 27$, $m/z = 81$ respectively), and calculated by normalising the impurity signal to both the argon carrier gas signal ($m/z = 36$) and mass of AB in the sample, smoothing the signal, then integrating the impurity release peak and taking the average value over three samples of the same composition (Fig. 7, Fig. S26).

This analysis shows that, diborane levels are unchanged in the composites compared to neat AB. Borazine is released at greater levels by the composites compared to neat AB, although the amount is negligible for AB10. The ammonia levels released by composites in the range AB60-AB90 are roughly the same as for neat AB, although as AB composition decreases, and there exists more intermediate phase relative to bulk AB in the composites, ammonia levels increase. This increase is significant in the case of AB10 and AB20, which do not contain bulk AB, suggesting that the low temperature hydrogen release reaction from the intermediate phase releases additional ammonia.

Hydrogen release mechanism from AB100

In order to gain insight into how the decomposition mechanism of AB in these materials differs from that of neat AB, *in-situ* $^{11}\text{B}\{^1\text{H}\}$ SS MAS-NMR experiments were performed whilst heating AB-PEO composites, and compared to the equivalent experiments on AB100 (Fig. 8, Fig. S27-36). This technique is very powerful, because the various boron environments in the species present have large chemical shifts, and spectra can be obtained quickly due to the high natural abundance of ^{11}B nuclei (80%) [37]. Many studies [5,23,37,40] have assigned the

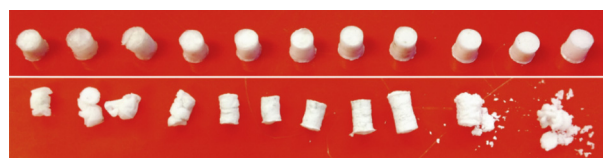


Fig. 6 – Appearance of 0.1 g pellets ranging from PEO (left) to AB (right), before (top) and after (bottom) the foam tests.

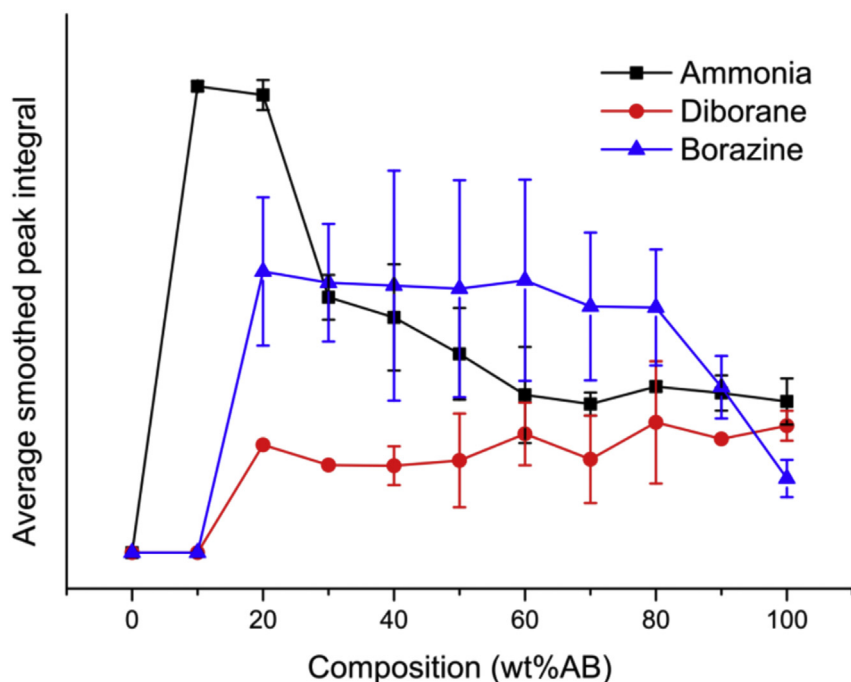


Fig. 7 – Average integrals of impurity release peaks shown in MS signals (error = standard deviation of 3 samples).

chemical shifts for the products and intermediates of dehydrogenation of AB. These data as well as the DSC and MS data already presented are used to describe the dehydrogenation of the AB-PEO materials.

The data for AB100 (Fig. 8a) show the formation of well-known reaction intermediates leading to hydrogen release. There are no obvious changes in the spectra when the material is heated from 25 °C to 95 °C, but at 105 °C the BH_3N signals for crystalline AB at –28 ppm and –25 ppm shift to a sharp peak at –23 ppm. This signal still represents a BH_3N moiety, but shifts as the result of a transition to a mobile phase of AB, commonly referred to as AB^* [41], where the dihydrogen bonding network of the AB crystal has been disrupted by heat. This leads to a different chemical environment for the AB molecules, hence the shift of the $^{11}\text{B}\{^1\text{H}\}$ SS MAS-NMR signal.

At 105 °C, there are signals at approximately –37 ppm and –13 ppm, indicating the formation of a BH_4^- ion and a linear BH_2N_2 environment respectively. These are indicative of the diammoniate of diborane (DADB, $[\text{NH}_3\text{BH}_2\text{NH}_3]^+[\text{BH}_4]^-$), an ionic species which is a precursor to hydrogen release from AB [37]. The slow formation of DADB by nucleation and growth is responsible for the long incubation period associated with hydrogen release from AB.

As the temperature continues to increase above 115 °C, new signals appear at –10 to –20 ppm and these increase in intensity at the expense of those from the BH_3N environment in AB^* . This is the result of a condensation reaction between the protic N–H moieties in the $[\text{NH}_3\text{BH}_2\text{NH}_3]^+$ cation of DADB and the hydridic B–H bonds in unreacted AB molecules to release hydrogen and form polymeric aminoborane (PAB) species, where the boron atoms are in sp^3 hybridised BH_2N_2 environments [23]. As the temperature increases further, these PAB species become branched and cross-linked,

indicated by signals at –6 ppm and 1 ppm representing sp [3] hybridised BHN_3 and BN_4 species respectively.

During the second hydrogen release step, at temperatures of ≈ 135 °C, signals at 27 and 31 ppm are seen, indicating sp [2] hybridised $\text{B}(-\text{NBH})_2(-\text{NB}_2)-$ and $\text{BH}(-\text{NBH})_2$ -like environments respectively. These species are highly cross-linked, indicated by the broadness of the $^{11}\text{B}\{^1\text{H}\}$ SS MAS-NMR signals. The reaction products from both AB100 and AB-PEO composites all resemble highly cross-linked polyborazylene-like materials (Fig. S37).

A broad, low intensity signal at –0.5 ppm can be also seen in the $^{11}\text{B}\{^1\text{H}\}$ SS MAS-NMR data for freeze-dried AB-PEO composites (Fig. S23), which may be either signal from an impurity in the as-received AB, or from a borate species (BO_2^-) arising from any hydrolysis of AB in the aqueous precursor solution prior to freeze-drying.

Hydrogen release mechanism from AB-PEO composites

For the AB-PEO composites, AB exists in two environments; in the intermediate phase and in the AB-rich phase. Therefore, AB30 (Fig. 8b) and AB70 (Fig. 8c) were probed using the in-situ $^{11}\text{B}\{^1\text{H}\}$ SS MAS-NMR technique to ascertain the dehydrogenation mechanisms for the intermediate phase and the bulk AB phase respectively.

Hydrogen release from the intermediate phase in AB-PEO composites

The evidence discussed thus far suggests that the low temperature hydrogen release reaction originates from the AB in the intermediate phase, and that this reaction releases more ammonia than the hydrogen release from bulk AB in the composites and AB100. The DSC data from AB10 and AB20

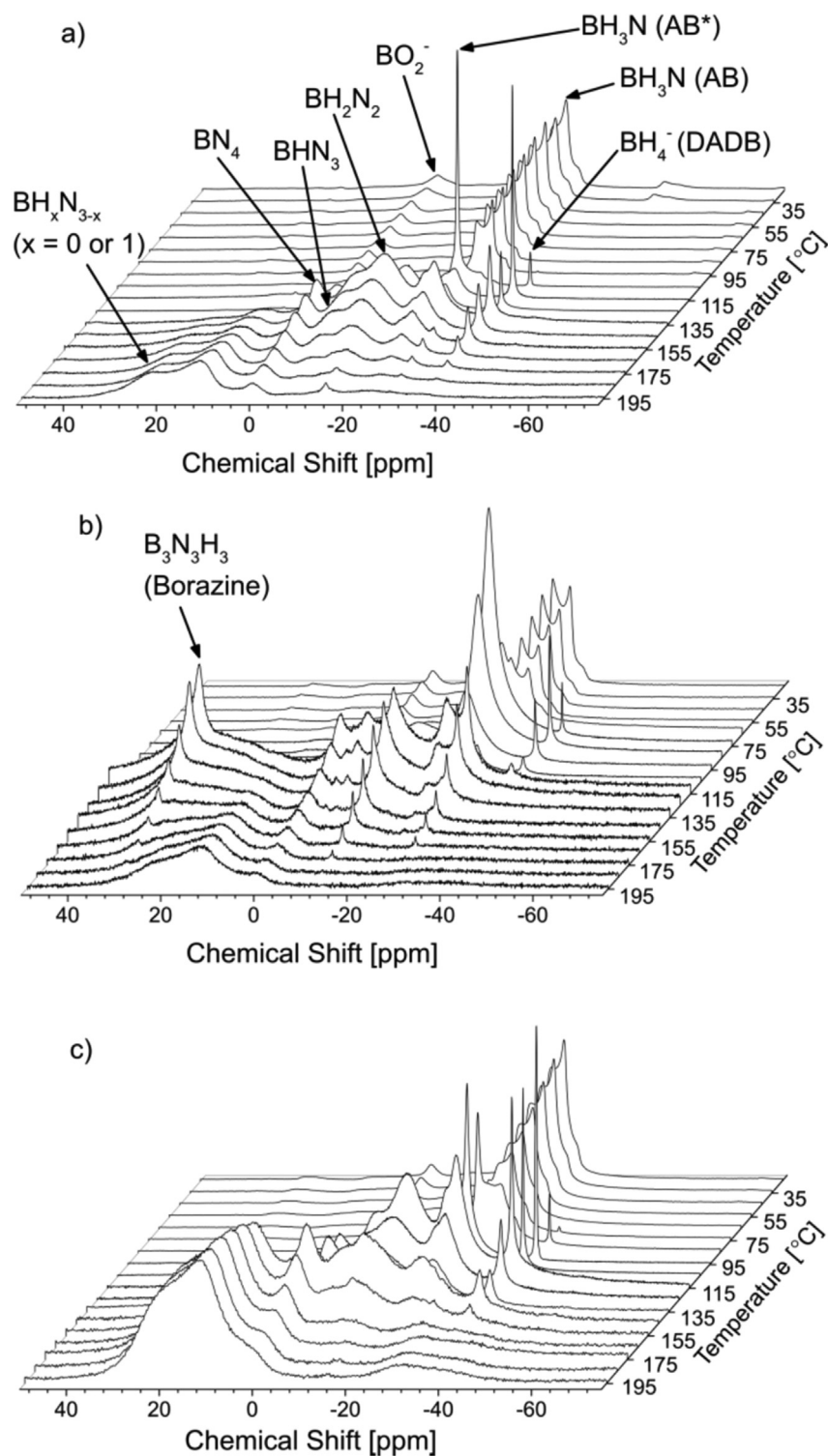


Fig. 8 – In-situ $^{11}\text{B}\{^1\text{H}\}$ SS MAS-NMR spectra for a) AB100, b) AB30 and c) AB70, heated at 1.2 °C/min.

(Fig. 4) show that the intermediate phase melts prior to the low temperature hydrogen release. As such, it is thought that the AB in the intermediate phase is effectively dissolved in a viscous PEO solution before and during its low temperature hydrogen release reaction. The hydrogen release mechanism suggested for the AB in the intermediate phase is described below (Fig. 9).

A recent study used both experimental and computational methods to show that polyethers promote the release of hydrogen from AB [42]. According to their density functional theory calculations, the interactions of the ethereal oxygen atom with the protic hydrogen atoms in the amine moiety of AB led to increased electron density in the AB molecule, with the effect of making the hydridic hydrogen atoms more

negatively charged. This increased charge results in greater nucleophilicity of the hydrides, which enhances the rate of hydride transfer required as the initial step in the formation of DADB, proceeding via the intermediate ammonia diborane (AaDB, $[\text{NH}_3\text{BH}_2(\mu\text{-H})\text{BH}_3]$) [43]. This is accompanied by the release of ammonia (NH_3), an impurity which was observed in the present study at this temperature in the MS data for low AB content composites (Fig. 7). This ammonia release is aided by the weakening of the B–N bond of the AB molecules, which become elongated when they are hydrogen bonded to polyethers, as calculated by Kim et al. [42] This free NH_3 can then attack the boron atom of AaDB to produce DADB.

In the *in-situ* $^{11}\text{B}\{^1\text{H}\}$ SS MAS-NMR data for AB30 (Fig. 8b), in which AB is thought to only exist in the intermediate phase, the formation of DADB is observed, but its existence is short-lived compared with the DADB signals for AB70 and AB100 (Fig. 8c and a), likely because the highly polar DADB is unstable in the PEO solution.

The decomposition of AB in polyethers is known to form borazine and related compounds. In fact, the most widely used synthetic procedures for the borazine production involve using polyethers as solvents [44,45]. The instability of DADB in polyethers leads to rapid oligomerisation, accompanied by hydrogen release. This decomposition results in the formation of small molecules with well-defined boron environments, which explains the sharpness of the peaks observed in the $^{11}\text{B}\{^1\text{H}\}$ SS MAS-NMR data in the present study (Fig. 8b). Although borazine's boiling point is 53°C , it is thought that the molten PEO could act as a solvent, coordinating to borazine molecules, and allowing for their detection in $^{11}\text{B}\{^1\text{H}\}$ SS MAS-NMR.

This evidence suggests that the AB within the intermediate phase undergoes the low-temperature dehydrogenation reaction due to the hydrogen bonds formed between the etheral oxygen atom ($-\text{O}-$) in the PEO backbone and the protic hydrogen atoms attached to the nitrogen atom ($\text{N}-\text{H}$) of AB molecules. Evidence for such interactions have been previously reported [1]. This interaction of AB with PEO is markedly different from that of AB with other polymers reported in the literature [24–27]. These other polymers contain carbonyl groups, which are thought to form B–O bonds with AB molecules during dehydrogenation, whereas there is no evidence for B–O bonds in the $^{11}\text{B}\{^1\text{H}\}$ SS MAS-NMR data for AB-PEO materials.

The main product of this reaction has been identified as B–(cyclotriborazanyl)amine-borane (BCTB) with signals at -24.0 , -11.2 , and -5.7 ppm, along with trace amounts of cyclotriborazane (CTB), seen as a shoulder to the main BCTB peak, at -12 ppm [46] (Fig. 8b). In addition, BHN_3 and BN_4 environments are present at -3 and 0 ppm respectively [47], indicating that the product species from these reactions are likely to be highly branched.

BCTB is an important intermediate in the dehydrogenation of AB in solution [46]. At 100°C , BCTB undergoes redistribution to form borazine and traces of CTB and AB without releasing hydrogen. This suggests that a 1,3-hydride transfer process from the BH_3 to the BH group of BCTB occurs, resulting in the formation of CTB and monomeric aminoborane (NH_2BH_2). Further hydrogen transfer processes then lead to the formation of borazine and AB, along with various intermediate species. This borazine signal is seen as a sharp peak in the ^{11}B

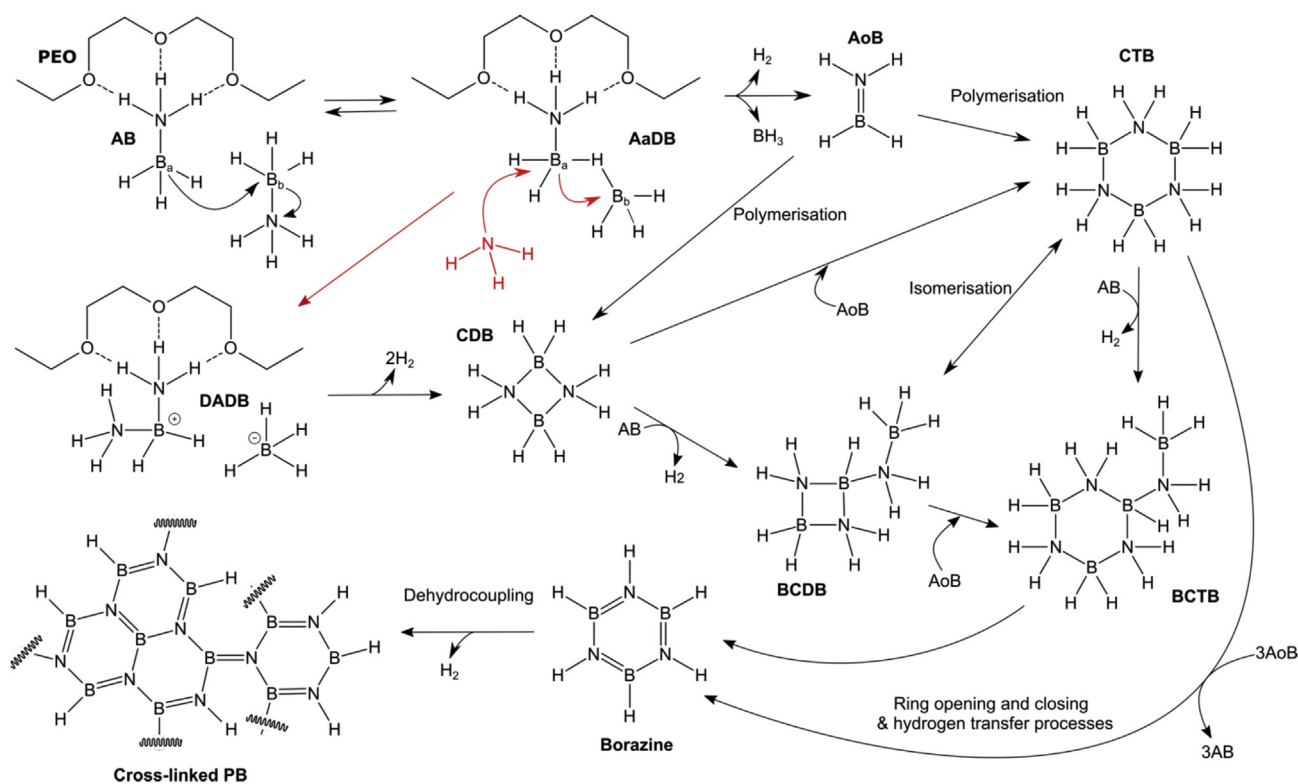


Fig. 9 – Suggested dehydrogenation mechanism of the AB in the intermediate phase, involving enhanced DADB formation due to hydrogen bonding interactions between the etheral oxygen atom ($-\text{O}-$) in the PEO backbone and the protic hydrogen atoms attached to the nitrogen atom ($\text{N}-\text{H}$) of AB molecules.

{¹H} SS MAS-NMR data (Fig. 8b). These reactions are exothermic but non-hydrogen producing, which explains the large exothermic peak at around 80 °C in Fig. 4 for AB20, and corresponding absence of a hydrogen peak at these temperatures in Fig. 5.

As the temperature increases, the borazine signals observed for AB30 decrease and we see signals reminiscent of polyborazylene (Fig. 8b). The dehydrocoupling of borazine to form polyborazylenes has been extensively studied [48,49]. No previous studies have observed such species or investigated the dehydrogenation of AB in polyethers at such high temperatures as this work.

Hydrogen release from bulk AB in AB-PEO composites

Hydrogen release from the bulk AB phase occurs by the same first and second hydrogen release steps as neat AB, seen as peaks at 106 °C and 147 °C in the MS data for the composites (Fig. 5), and also as exothermic signals in the DSC data (Fig. 4) at the same temperatures. However, the bulk AB is also in contact with PEO at the interface between bulk AB regions and the intermediate phase regions. As such, it is thought the polyether-mediated mechanism described for the intermediate phase (Fig. 9) acts to reduce the activation barrier to DADB formation at the AB-intermediate phase interface, resulting in the supply of nucleation sites for DADB, which subsequently nucleates and grows, followed by dehydrogenation by the well-known route (Fig. 10). There is evidence for this catalysed DADB formation in the ¹¹B{¹H} SS MAS-NMR data (Fig. 8c), as well as the reduction in the hydrogen release temperatures of the first and second hydrogen release steps from the AB-PEO

materials compared to neat AB seen in the DSC (Fig. 4) and MS (Fig. 5) data.

Phase diagram

All of the evidence from this study, as well as some additional samples in the low-AB composition region (Fig. S38), have been combined to suggest a temperature-composition phase diagram for AB-PEO (Fig. 11). The onset temperatures of the hydrogen release steps have been calculated from DSC data using a two tangent method (Fig. S39) and overlaid.

For AB40-AB90, the onset of the low temperature hydrogen release coincides with the melting of the intermediate phase, as does the first hydrogen release step with the melting of the bulk AB phase, supporting the proposed hydrogen release mechanisms above. In contrast to bulk AB, AB molecules in the intermediate phase are not thought to be bonded together by di-hydrogen bonds, rather, they are believed to be involved in hydrogen bonding to the –O– in the PEO backbone. Therefore it is likely that the intermediate phase must melt in order to allow the diffusion and interaction of adjacent AB molecules to begin hydrogen release.

For compositions below AB30, where all of the AB molecules are in the intermediate phase, the onset of hydrogen release is at significantly higher temperatures than the melting of PEO and the intermediate phase. Unlike for AB40-AB90, for AB20, the first phase to melt is PEO, and the low hydrogen release from AB in the mixed phase only comes at temperatures approaching the melting of the intermediate phase. The two-step dehydrogenation follows in the liquid state.

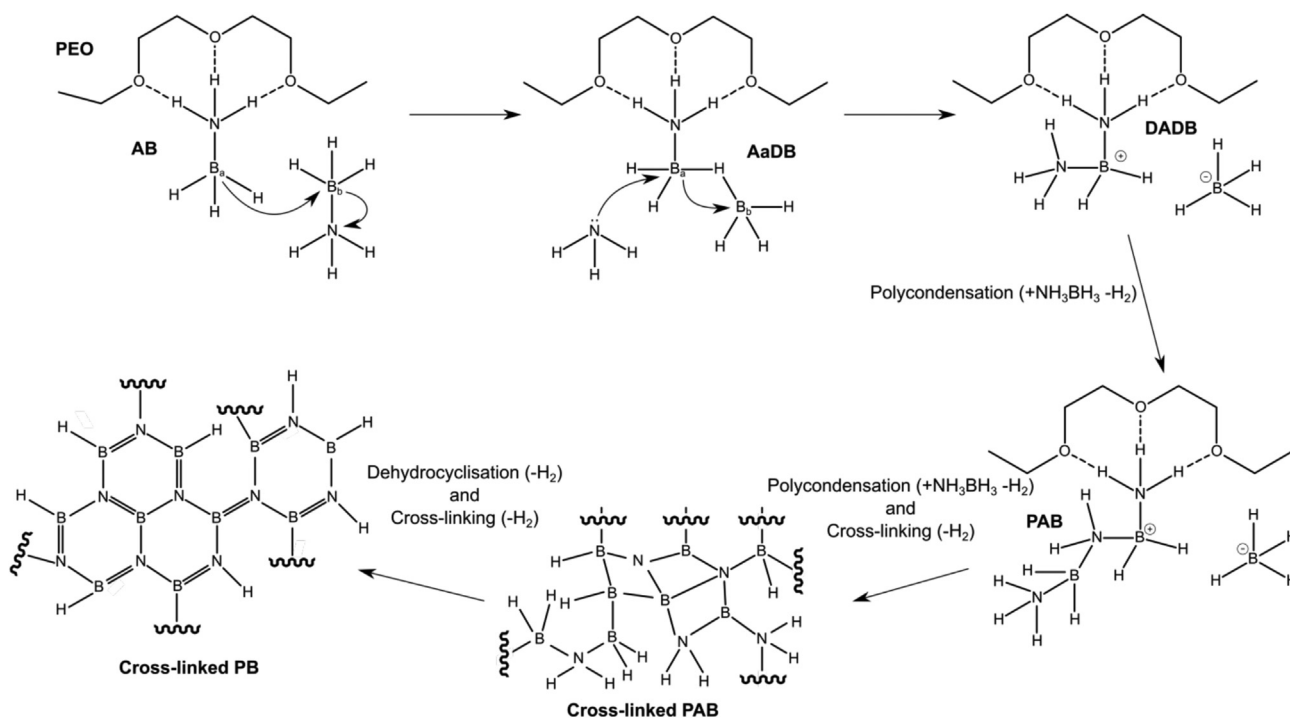


Fig. 10 – Suggested dehydrogenation mechanism of the bulk AB in AB-PEO composites at compositions above AB30. At the interface of bulk AB and the intermediate phase, the PEO in the intermediate phase helps to promote the formation of DADB, which then follows the well-known dehydrogenation mechanism for AB by polycondensation, cross-linking and dehydrocyclisation reactions.

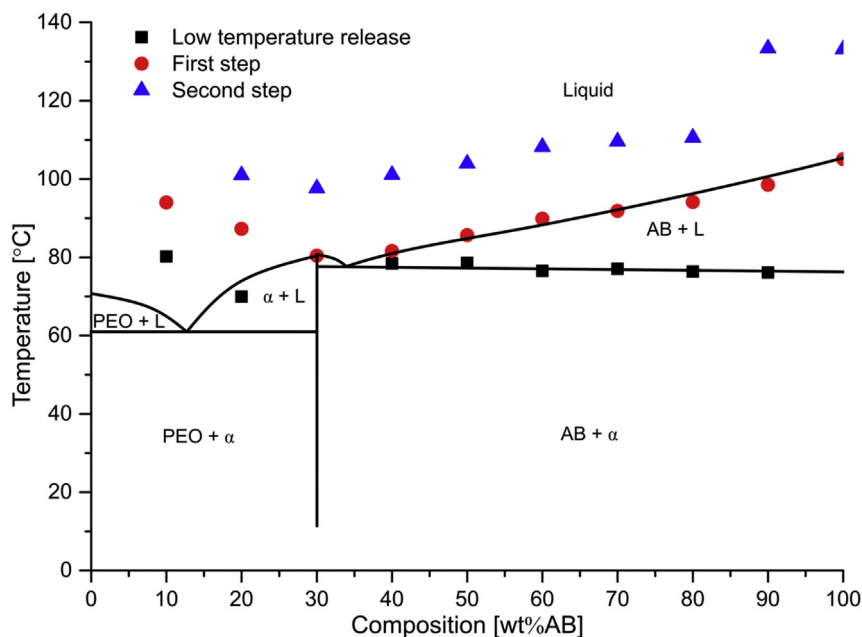


Fig. 11 – Temperature-composition phase diagram for the AB-PEO system, including the temperature of the onset of hydrogen release reactions. α = intermediate phase.

For AB10, the intermediate phase melts first, followed by PEO, and hydrogen release comes at higher temperatures in the liquid state. It is possible that, being so dilute in AB molecules, more energy is required for the diffusion of AB molecules such that they can encounter and interact with each other in sufficient concentration for dehydrogenation reactions to occur.

Suppression of foaming

The phase mixing and hydrogen release behaviour already discussed, can explain why PEO is so effective at reducing the foaming of AB during hydrogen release.

The low temperature hydrogen release from the intermediate phase helps to reduce foaming. This reaction produces highly cross-linked solid materials, prior to and during, the first hydrogen release step from bulk AB. It is likely that these products act to hold the pelletised material together during the first and second hydrogen release steps.

Furthermore, although PEO and the intermediate phase are molten prior to hydrogen release, the high molecular weight PEO is still an extremely viscous fluid. This high viscosity helps to resist expansion of the material during hydrogen release, disrupting bubble formation and therefore inhibiting the foaming of AB.

The porous macrostructure produced by freeze-drying AB-PEO composites from aqueous solution allows for their easy pressing into dense cylindrical pellets. Comparing the pellets before and after the foam tests shows that they appear to increase in height during hydrogen release, and some delaminated regions can be seen (Fig. 6). As the material is loaded into the die, it becomes folded, and these folds must form weaknesses in the pellet once pressed which delaminate during hydrogen release. It is likely that these regions

become the path of least resistance for hydrogen produced inside the pellets, helping to reduce unwanted pressure build-up by allowing for quick diffusion and liberation of hydrogen gas.

Conclusions

It has been shown that producing AB-PEO materials by freeze-drying from aqueous solutions achieves intimate mixing similar to that obtained in our previous work using co-electrospinning [1], with the benefits of a robust processing route with great potential for materials production at an industrial scale.

The reaction of AB and PEO when mixed in this way forms an intermediate phase which is phase-pure at 30 wt% AB, with a distinct crystal structure. This phase is suggested to dehydrogenate through solution-state processes as a result of the molten PEO acting as a solvent for AB. Hydrogen bonding interactions between the etheral oxygen atom ($-O-$) in the PEO backbone and the protic hydrogen atoms attached to the nitrogen atom ($N-H$) of AB molecules promote the formation of DADB, resulting in a low temperature hydrogen release reaction unique to this phase.

For composites AB40-AB90, AB exists in bulk, and releases hydrogen through well-known two-step dehydrogenation mechanisms below 200 °C. In the AB-PEO composites it is suggested that the reduction in dehydrogenation temperature of the two-step process is due to an enhanced rate of DADB formation at the interface between the intermediate phase and bulk AB due to the same hydrogen bonding interaction between the etheral oxygen atom ($-O-$) in the PEO backbone and the protic hydrogen atoms attached to the nitrogen atom ($N-H$) of AB molecules.

A temperature-composition phase diagram has been produced to summarise the close relationship between phase mixing behaviour and hydrogen release of these unique composites.

PEO acts to eliminate foaming of AB due to the high viscosity of the molten PEO-containing phases and the early formation of polymeric by-products. Furthermore, delaminated regions running across the pellets are suggested to provide the path of least resistance for hydrogen released from within.

The elimination of foaming by AB-PEO freeze-dried composites, combined with favourable hydrogen release temperatures, facile production and high gravimetric and volumetric hydrogen capacity makes this solid-state hydrogen storage material a promising candidate for wide-spread portable hydrogen-powered systems.

Acknowledgements

The authors wish to thank Dr Arthur Lovell, Dr Joseph Cook and Dr James Wilgeroth of Cella Energy for their contributions to this work. We would like to thank Dr Marek Jura and Dr Gavin Stenning for help with the *in-situ* XRD experiments carried out on the Rigaku XRD instrument in the Materials Characterisation Laboratory at the ISIS Neutron and Muon Source, Oxfordshire. This work was supported by the EPSRC [grant EP/L015862/1 “EPSRC Centre for Doctoral Training in Molecular Modelling and Materials Science”] and Cella Energy.

Appendix A. Supplementary data

Supplementary data related to this article can be found at <https://doi.org/10.1016/j.ijhydene.2018.01.128>.

REFERENCES

- Nathanson A, Ploszajski A, Billing M, Cook J, Jenkins D, Headen T, et al. Ammonia borane–polyethylene oxide composite materials for solid hydrogen storage. *J Mater Chem A* 2015;3:3683–91.
- Summerscales OT, Gordon JC. Regeneration of ammonia borane from spent fuel materials. *Dalton Trans* 2013;42:10075–84.
- Mayer E. Symmetrical cleavage of diborane by ammonia in solution. *Inorg Chem* 1972;11:866–9.
- Lai S-W, Lin H-L, Yu TL, Lee L-P, Weng B-J. Hydrogen release from ammonia borane embedded in mesoporous silica scaffolds: SBA-15 and MCM-41. *Int J Hydrogen Energy* 2012;37:14393–404.
- Sepehri S, Feaver A, Shaw WJ, Howard CJ, Zhang Q, Autrey T, et al. Spectroscopic studies of dehydrogenation of ammonia borane in carbon cryogel. *J Phys Chem B* 2007;111:14285–9.
- Tang Z, Chen H, Chen X, Wu L, Yu X. Graphene oxide based recyclable dehydrogenation of ammonia borane within a hybrid nanostructure. *J Am Chem Soc* 2012;134:5464–7.
- Moussa G, Bernard S, Demirci UB, Chiriac R, Miele P. Room-temperature hydrogen release from activated carbon-confined ammonia borane. *Int J Hydrogen Energy* 2012;37:13437–45.
- Li SF, Guo YH, Sun WW, Sun DL, Yu XB. Platinum nanoparticle functionalized CNTs as nanoscaffolds and catalysts to enhance the dehydrogenation of ammonia-borane. *J Phys Chem C* 2010;114:21885–90.
- Moussa G, Demirci UB, Malo S, Bernard S, Miele P. Hollow core@mesoporous shell boron nitride nanopolyhedron-confined ammonia borane: a pure B–N–H composite for chemical hydrogen storage. *J Mater Chem A* 2014;2:7717–22.
- Gutowska A, Li L, Shin Y, Wang CM, Li XS, Linehan JC, et al. Nanoscaffold mediates hydrogen release and the reactivity of ammonia borane. *Angew Chem Int Ed* 2005;44:3578–3382.
- Kalidindi SB, Joseph J, Jagirdar BR. Cu²⁺-induced room temperature hydrogen release from ammonia borane. *Energy Environ Sci* 2009;2:1274–6.
- He T, Xiong Z, Wu G, Chu H, Wu C, Zhang T, et al. Nanosized Co- and Ni-Catalyzed ammonia borane for hydrogen storage. *Chem Mater* 2009;21:2315–8.
- Li Y, Fang F, Song Y, Li Y, Zhang Q, Ouyang L, et al. Enhanced dehydrogenation of ammonia borane by reaction with alkaline earth metal chlorides. *Int J Hydrogen Energy* 2012;37:4274–9.
- Graham KR, Kemmitt T, Bowden ME. High capacity hydrogen storage in a hybrid ammonia borane–lithium amide material. *Energy Environ Sci* 2009;2:706–10.
- Dovgaliuk I, Le Duff CS, Robeyns K, Devillers M, Filinchuk Y. Mild dehydrogenation of ammonia borane complexed with aluminum borohydride. *Chem Mater* 2015;27:768–77.
- Wang YW, Guo ZX. Enhanced hydrogen desorption of an ammonia borane and lithium hydride system through synthesised intermediate compounds. *J Mater Chem A* 2014;2:6801–13.
- Wu H, Zhou W, Pinkerton FE, Meyer MS, Srinivas G, Yildirim T, et al. A new family of metal borohydride ammonia borane complexes: synthesis, structures, and hydrogen storage properties. *J Mater Chem* 2010;20:6550–6.
- Gangal AC, Kale P, Edla R, Manna J, Sharma P. Study of kinetics and thermal decomposition of ammonia borane in presence of silicon nanoparticles. *Int J Hydrogen Energy* 2012;37:6741–8.
- Gangal AC, Edla R, Iyer K, Biniwale R, Vashistha M, Sharma P. Effect of zeolites on thermal decomposition of ammonia borane. *Int J Hydrogen Energy* 2012;37:3712–8.
- Choi YJ, Rönnebro ECE, Rassat S, Karkamkar A, Maupin G, Holladay J, et al. Kinetics study of solid ammonia borane hydrogen release - modeling and experimental validation for chemical hydrogen storage. *Phys Chem Chem Phys* 2014;16:7959–68.
- Hwang HT, Greenman P, Kim SJ, Varma A. Effect of boric acid on thermal dehydrogenation of ammonia borane: H₂ yield and process characteristics. *Am Inst Chem Eng* 2013;59:405–10.
- Himmelberger DW, Alden LR, Bluhm ME, Sneddon LG. Ammonia borane hydrogen release in ionic liquids. *Inorg Chem* 2009;48:9883–9.
- Heldebrant DJ, Karkamkar A, Hess NJ, Bowden M, Rassat S, Zheng F, et al. The effects of chemical additives on the induction phase in solid-state thermal decomposition of ammonia borane. *Chem Mater* 2008;20:5332–6.
- Zhao J, Shi J, Zhang X, Cheng F, Liang J, Tao Z, et al. A soft hydrogen storage material: poly(methyl acrylate)-confined ammonia borane with controllable dehydrogenation. *Adv Mater* 2010;22:394–7.
- Alipour J, Shoushtari A, Kafrou A. Ammonia borane confined by poly(methyl methacrylate)/multiwall carbon nanotube nanofiber composite, as a polymeric hydrogen storage material. *J Mater Sci* 2015;50:3110–7.

- [26] Tang Z, Li S, Yang Z, Yu X. Ammonia borane nanofibers supported by poly(vinyl pyrrolidone) for dehydrogenation. *J Mater Chem* 2011;21:14616–21.
- [27] Li SF, Tang ZW, Tan YB, Yu XB. Polyacrylamide blending with ammonia borane: a polymer supported hydrogen storage composite. *J Phys Chem C* 2012;116:1544–9.
- [28] Bowden ME, Gainsford GJ, Robinson WT. Room-temperature structure of ammonia borane. *Aust J Chem* 2007;60:149–53.
- [29] Takahashi Y, Tadokoro H. Structural studies of polyethers, $-(\text{CH}_2)_m\text{-O-})_n$. X. Crystal structure of poly(ethylene oxide). *Macromolecules* 1973;6:672–5.
- [30] Shirley R. CRYSFIRE Suite: The CRYSFIRE System for Automatic Powder Indexing. <http://www.ccp14.ac.uk/tutorial/crys/>.
- [31] Visser JW. A fully automatic program for finding the unit cell from powder data. *J Appl Crystallogr* 1969;2:89–95.
- [32] Laugier J, Bochu B. LMGP-suite of programs for the interpretation of X-ray experiments. 2000. <http://www.ccp14.ac.uk/tutorial/lmgp/>.
- [33] Hunter B. Rietica – a visual Rietveld program. 1998. <http://www.rietica.org/>.
- [34] Chung FH. Quantitative interpretation of X-ray diffraction patterns of mixtures. I. Matrix-flushing method for quantitative multicomponent analysis. *J Appl Crystallogr* 1974;7:519–25.
- [35] Le Bail A, Duroy H, Fourquet JL. Ab initio structure determination of LiSbWO_6 by X-ray powder diffraction. *Mater Res Bull* 1988;23:447–52.
- [36] Scarlett NVY, Madsen IC. Quantification of phases with partial or no known crystal structures. *Powder Diffr* 2006;21:278–84.
- [37] Stowe AC, Shaw WJ, Linehan JC, Schmid B, Autrey T. In situ solid state ^{11}B MAS-NMR studies of the thermal decomposition of ammonia borane: mechanistic studies of the hydrogen release pathways from a solid state hydrogen storage material. *Phys Chem Chem Phys* 2007;9:1831–6.
- [38] Stephens FH, Pons V, Baker RT. Ammonia-borane: the hydrogen source par excellence? *Dalton Trans* 2007;2: 2613–26.
- [39] Frueh S, Kellett R, Mallery C, Molter T, Willis WS, King'Ondu C, et al. Pyrolytic decomposition of ammonia borane to boron nitride. *Inorg Chem* 2011;50:783–92.
- [40] Bluhm ME, Bradley MG, Butterick III R, Kusari U, Sneddon LG. Amineborane-based chemical hydrogen Storage: enhanced ammonia borane dehydrogenation in ionic liquids. *J Am Chem Soc* 2006;128:7748–9.
- [41] Shaw WJ, Bowden M, Karkamkar A, Howard CJ, Heldebrant DJ, Hess NJ, et al. Characterization of a new phase of ammonia borane. *Energy Environ Sci* 2010;3:796–804.
- [42] Kim Y, Baek H, Lee JH, Yeo S, Kim K, Hwang S-J, et al. Metal-free, polyether-mediated H_2 -release from ammonia borane: roles of hydrogen bonding interactions in promoting dehydrogenation. *Phys Chem Chem Phys* 2013;15:19584–94.
- [43] Chen X, Bao X, Zhao J, Shore SG. Experimental and computational study of the formation mechanism of the diammoniate of diborane: the role of dihydrogen bonds. *J Am Chem Soc* 2011;133:14172–5.
- [44] Wideman T, Sneddon LG, Widman T, Sheddon LG. Convenient procedures for the laboratory preparation of borazine. *Inorg Chem* 1995;34:1002–3.
- [45] Li J, Zhang C, Li B, Cao F, Wang S. An investigation on the synthesis of borazine. *Inorg Chim Acta* 2011;366:173–6.
- [46] Kalviri HA, Gärtner F, Ye G, Korobkov I, Baker RT. Probing the second dehydrogenation step in ammonia-borane dehydrocoupling: characterization and reactivity of the key intermediate, B-(cyclotriborazanyl)amine-borane. *Chem Sci* 2015;6:618–24.
- [47] Kobayashi T, Gupta S, Caporini MA, Pecharsky VK, Pruski M. Mechanism of solid-state thermolysis of ammonia borane: a ^{15}N NMR study using fast magic-angle spinning and dynamic nuclear polarization. *J Phys Chem C* 2014;118:19548–55.
- [48] Li J, Bernard S, Salles V, Gervais C, Miele P. Preparation of polyborazylene-derived bulk boron nitride with tunable properties by warm-pressing and pressureless pyrolysis. *Chem Mater* 2010;22:2010–9.
- [49] Bernard S, Miele P. Polymer-derived boron nitride: a review on the chemistry, shaping and ceramic conversion of borazine derivatives. *Materials Basel* 2014;7:7436–59.